GEOSTANDARDS and GEOANALYTICAL RESEARCH

Precise Measurement of Magnesium Isotopes in Fe-Mg Minerals Using a Multi-collector SHRIMP Ion Microprobe

Fernando **Bea** (1)*, Pilar **Montero** (1), Delia **Ortega** (2), José F. **Molina** (1), Aitor **Cambeses** (1), Leticia **Barcos** (1), Shui-Jiong **Wang** (3) and Shan **Ke** (3)

(1) Department of Mineralogy and Petrology, University of Granada, Campus Fuentenueva, 18002, Granada, Spain
(2) Centro de Instrumentación Científica, University of Granada, Campus Fuentenueva, 18002, Granada, Spain
(3) State Key Laboratory of Geological Processes and Mineral Resources, China University of Geosciences, Beijing 100083, China
* Corresponding author. e-mail: fbea@ugr.es

The distribution of Mg isotopes in minerals is becoming increasingly relevant in Earth science. Usually, they are determined by dissolving mineral concentrates and, after purifying Mg with ion exchange resins, analysing the resulting solutions by TIMS or, most often, MC-ICP-MS. When applied to individual minerals, these methods are slow and prone to contamination from impurities in the concentrates, inconveniences that may be avoided using spot analysis techniques such as LA-MC-ICP-MS or SIMS, albeit at the price of a large instrumental mass fractionation (IMF) and isobaric interferences, most prominent in the former. Here, we studied the potential of the multi-collector SHRIMP II ion microprobe for measuring Mg isotopes in Fe-Mg silicates and oxides. We found that, when corrected for the divergence of the Mg ion paths within the sample chamber caused by the Earth's magnetic field, the SHRIMP's IMF overwhelmingly depends on the mineral species, and the effects of variable chemical composition are negligible. We propose that the IMF is caused by the *force constant difference*, ΔF, between "hard" and "soft" bonds linking the ions of the studied element to the mineral lattice. Given that ΔF is a constant for each mineral species, we calculated IMF-correction factors for the most common Mg-bearing minerals. The thus-calculated correction factors permit the analysis in the same session, and with reasonable accuracy (within ~0.3‰ of the δ^{26}Mg determined by SN-MC-ICP-MS analyses of concentrates), of samples from different mineral species, facilitating the application of Mg isotopes to terrestrial studies.

Keywords: ion microprobe, Mg isotopes, mass fractionation, matrix effects, correction factors.

Received 05 Nov 23 – Accepted 08 Feb 24

After oxygen, magnesium is the most abundant element in the solid Earth; it has three isotopes, ^{24}Mg, ^{25}Mg and ^{26}Mg, with molar fractions of 0.78992, 0.10003 and 0.11005, whose relative abundances are expressed as delta values:

$$\delta^{xx}Mg = \left[\left(^{xx}Mg/^{24}Mg_{sample}\right)/\left(^{xx}Mg/^{24}Mg_{reference}\right)-1\right] \quad (1)$$

where xx is either 25 or 26, and the reference value is from the DMS3 reference material (^{25}Mg/^{24}Mg = 0.126851; ^{26}Mg/^{24}Mg = 0.139796: Galy *et al.* 2003, Young and Galy 2004).

In the three-isotope diagram (δ^{25}Mg *vs.* δ^{26}Mg, Figure 1), materials fractionated from a uniform reservoir define a straight line:

$$\delta^{25}Mg = ß \times \delta^{26}Mg \quad (2)$$

the theoretical slope of which ranges between ß = 0.500 and ß = 0.521, depending on the mass fractionation law chosen (Davis *et al.* 2015). All terrestrial and most meteoritic materials plot along a line with slope between ß = 0.511 and 0.521 corresponding to the predicted equilibrium and kinetic mass fractionation laws (Galy *et al.* 2001, 2003, Young and Galy 2004), which is duly called the *terrestrial*

doi: 10.1111/ggr.12547

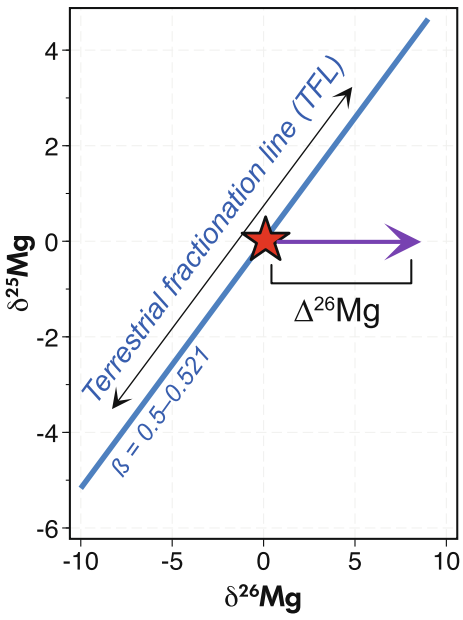

Figure 1. The three Mg isotopes diagram. The *terrestrial fractionation line* (TFL) has a theoretical slope between 0.500 and 0.521, depending on the fractionation model chosen; it is straight except if the mass fractionation law chosen is linear (Davis *et al.* 2015). $\Delta^{26}Mg = \delta^{26}Mg_{measured} - \beta^{-1}\,\delta^{25}Mg_{measured}$ represents the excess of radiogenic ^{26}Mg attributed to the decay ^{26}Al isotope, characteristic of Al-rich meteoritic materials accreted soon after the Solar nucleosynthesis (see text for details). Terrestrial materials mostly plot along the TFL; unfortunately, instrumental mass fractionation also causes variations along the TFL, which, if uncorrected, mask the effects of geological processes. The star represents Bulk Earth's composition.

fractionation line (TFL). Some meteoritic materials, especially the CAIs, fall to the right because they contain radiogenic ^{26}Mg (Gray and Compston 1974, Lee and Papanastassiou 1974). The excess ^{26}Mg (Figure 1) is usually reported as $\Delta^{26}Mg = \delta^{26}Mg_{measured} - \delta^{25}Mg_{measured}\,\beta^{-1}$ and generally attributed to the decay of the high heat-producing and short-lived ^{26}Al isotope, incorporated only in minerals accreted early during the condensation of the Solar nebula.

The first bulk measurements of Mg isotopes were done with thermal ionisation mass spectrometry (TIMS) on dissolved – and ion exchange purified – rock samples and mineral concentrates (*op. cit.*). The first spot analyses of minerals were done with secondary ion mass spectrometry (SIMS) using single-collector and relatively simple ion microprobes such as the Chicago AEI IM-20 (e.g., Hutcheon *et al.* 1978, Russell *et al.* 2000, Richter *et al.* 2002) or the Canberra SHRIMP I (Ireland *et al.* 1986). Both TIMS and SIMS produced a large instrumental mass fractionation (IMF) so that the resulting $^{25}Mg/^{24}Mg$ was normalised to a reference value of 0.12663, then believed to approximate the Earth's mean (Catanzaro *et al.* 1966), and the measured $^{26}Mg/^{24}Mg$ ratios were duly corrected according to the exponential law of mass fractionation:

$$^{26}Mg/^{24}Mg_{corrected} = [0.12663/(^{25}Mg/^{24}Mg_{measured})]^2 \times {}^{26}Mg/^{24}Mg_{measured} \quad (3)$$

which yielded values of $\Delta^{26}Mg$ that are precise enough for meteoritic studies. However, the lack of a suitable method for correcting the IMF and the subsequent necessity of normalisation prevented studying the Mg isotope fractionation occurring in geological processes, that is, to determine the position along the TFL (see Figure 1). Such studies were only possible with the development of multi-collector (MC) ICP-MS because this technique, when operating in solution-nebulisation mode (SN-MC-ICP-MS) causes a uniform instrumental mass fractionation, which is easily correctable (Young and Galy 2004, and references therein). Determining Mg isotopes after dissolving the sample also permits separating the matrix components and potential interferents with ion-exchange resins before analyses.

SN-MC-ICP-MS copes well with bulk-rock analysis but not with individual minerals because it is time-consuming, lacks spatial resolution and is prone to contamination by impurities within the mineral concentrates. These disadvantages are suppressed by analysing spots of solid mineral grains with laser ablation (LA) MC-ICP-MS or SIMS (see revision in Chaussidon *et al.* 2017), albeit at the price of introducing new drawbacks, such as large and variable IMF and potential isobaric interferences.

Magnesium isotope measurement using large-radius ion microprobes suffer from little, if any, isobaric interferences, especially if cryogenic pumps evacuate the sample chamber until a vacuum is in the E^{-08} Torr range, but have a large IMF, the causes of which are still poorly understood (see references below). In principle, we can consider the IMF as consisting of two components: one related to the mineral lattice and the other related to the chemical composition of a given mineral. The former occurs when reference materials and unknowns belong to different mineral species. The latter occurs when reference materials and unknowns belong to the same mineral species but have different compositions. Ireland *et al.* (1986), using a single collector SHRIMP I ion

microprobe, considered only the different-mineral effect and proposed IMF correction factors relative to kaersutite, which they used as a reference material. In contrast, authors working with multi-collector ion microprobes (CAMECA 1270 and 1280, e.g., Kita *et al.* 2012, Luu *et al.* 2013, Ushikubo *et al.* 2013, Fukuda *et al.* 2020, Richter *et al.* 2021) have repeatedly reported IMF effects for the same mineral species that depend on the chemical composition, proposing corrections equations derived from reference materials of known Mg isotope ratios and variable chemical compositions.

Preliminary work with the Granada MC SHRIMP IIe has shown that the chemical composition-related IMF is negligible in the single-collection mode, confirming the result of Ireland *et al.* (1986), but it may be noticeable in the multi-collection mode. Multi-collection is inherently more precise than single collection and, therefore, highly desirable for precise measurement of Mg isotopes. For this reason, we undertook a study to understand the reasons for the instrumental mass fractionation of Mg isotopes in the MC SHRIMP and how it might be corrected for olivine, clinopyroxene, orthopyroxene, amphibole, spinel, garnet, cordierite and biotite, the results of which are reported here. We found that if the local effects of the Earth's magnetic field on the Mg isotopes ionic paths within the sample chamber are well corrected, the IMF overwhelmingly depends on the differences in the mineral nature. This observation permitted us to calculate IMF correction factors for the minerals mentioned above, enabling reasonably accurate determination of Mg isotopes in different minerals using a single reference material instead of employing a different reference material for each mineral species and then correcting the results according to its specific chemical composition.

Materials and methods

For this study, we used nineteen mineral concentrates: (i) San Carlos peridotite olivine, clinopyroxene, orthopyroxene and spinel (Hu *et al.* 2016), (ii) Ronda peridotite olivine, clinopyroxene, orthopyroxene and spinel (Garrido *et al.* 2011), (iii) olivine, clinopyroxene, orthopyroxene and amphibole from a high-*T* mafic granulite of the Adrar Stuff metamafic complex (Molina *et al.* 2018), the bulk-rock Mg isotope composition if which was previously known, and (iv) gem-quality crystals from different localities: olivine, garnet, cordierite, orthopyroxene, clinopyroxene, amphibole and biotite.

After dissolution and chromatographic purification, the six gem-quality minerals and the Ronda peridotite minerals were analysed using MC-ICP-MS. The Adrar Sutuff granulite minerals were not analysed in this way. However, we included them in the study because their bulk composition differs substantially from the peridotitic minerals; they likely have identical Mg isotope ratios because of diffusion after being equilibrated at $T \geq 1000$ °C (Molina *et al.* in review, Molina *et al.* 2018) and the Mg isotope bulk-rock composition was known.

To assess the influence of the bulk chemical composition, Fe mainly, on the instrumental mass fractionation of Mg isotopes, we made three synthetic glasses with identical Mg isotope ratios, similar MgO mass fraction (~ 5% *m/m*) and different FeO (0, 5 and 10% *m/m*), with the remaining elements varying concomitantly. The compositions of all studied materials, glasses and minerals are given in Table 1.

Sample preparation and SHRIMP analysis

Handpicked mineral grains were mounted with high-vacuum epoxy in a SHRIMP megamount. These were 35 mm in diameter and were screwed from their back in the mount holder to avoid metal and abrupt topographic changes facing the extraction plate. This configuration was designed by Ickert *et al.* (2008) to minimise the fractionation of oxygen isotopes during the extraction of secondary ions in grains located off-centre of the mount.

Once mounted and polished, mineral grains were studied by optical and SEM microscopy to detect cracks and inclusions, and then coated with a 10 nm thick gold layer to be analysed in the SHRIMP IIe/mc ion microprobe at the IBERSIMS laboratory of the CIC-University of Granada, Spain. The primary beam was composed of $^{16}O^{16}O^-$, filtered with a Wien mass filter and set to a yield of ≈ 6 nA. The primary ion optics were configured with a 120 µm Kohler aperture to produce a ~ 18 µm diameter spot on the megamount surface. The secondary beam was guided through the 100-µm source slit to the electrostatic analyser, maximising its signal of the post-ESA monitor. From here, the secondary beam was focused and guided with the post-ESA quadrupole to the collector through the magnet. The collector consisted of three Faraday cups arranged to detect each Mg isotope peak at the same magnetic field, yielding precisely matched peak shapes. Additionally, their 200 µm entrance slits were moved vertically so that the vertical scanning of the secondary beam with the post-ESA quadrupole produced matched patterns for the three cups. The ion current arriving at the Faraday cups was measured with e7600 electrometers designed around Thermo Finnigan DC amplifier modules. The electrometers were set with

Table 1.
Phases used in this study

Phase	ID	Extracted from	FeO_t	MgO	#Mg	$\partial^{26}Mg$	Reference
Olivine	OLsc	San Carlos peridotite	10.10	49.91	0.90	-0.24	Hu *et al.* (2016)
Orthopyroxene	OPXsc	San Carlos peridotite	5.83	34.00	0.91	-0.22	Hu *et al.* (2016)
Clinopyroxene	CPXsc	San Carlos peridotite	2.47	16.34	0.92	-0.23	Hu *et al.* (2016)
Spinel	SPsc	San Carlos peridotite	12.66	18.03	0.72	-0.23	Hu *et al.* (2016)
Olivine	OLro	Ronda peridotite	9.33	44.50	0.89	-0.22	this work
Orthopyroxene	OPXro	Ronda peridotite	6.66	33.76	0.90	-0.21	this work
Clinopyroxene	CPXro	Ronda peridotite	2.35	15.30	0.92	-0.14	this work
Spinel	SPro	Ronda peridotite	12.06	19.38	0.74	0.28	this work
Olivine	OLas	Adrar Sutuff high-*T* granulite	29.02	34.19	0.68	n.d*	Molina *et al.* (2018)
Orthopyroxene	OPXas	Adrar Sutuff high-*T* granulite	16.81	26.29	0.74	n.d*	Molina *et al.* (2018)
Clinopyroxene	CPXas	Adrar Sutuff high-*T* granulite	6.95	14.79	0.79	n.d*	Molina *et al.* (2018)
Amphibole	AMPas	Adrar Sutuff high-*T* granulite	9.43	13.70	0.72	n.d*	Molina *et al.* (2018)
Olivine	OLf	unknown	9.90	50.08	0.90	-0.21	this work
Cordierite	CRD	unknown	3.48	12.37	0.86	-0.54	this work
Cannilloite	CAN	Adrar Sutuff pegmatite	12.44	14.87	0.68	-0.30	this work
Orthopyroxene	OPX7	unknown	7.08	35.56	0.90	-0.67	this work
Clinopyroxene	CPX2	unknown	2.90	16.56	0.91	-1.88	this work
Garnet	GRTf	Lapland granulite	37.42	3.00	0.13	-1.37	this work
Biotite	BT35	unknown	22.53	10.45	0.45	-0.11	this work
Glass 1	KFS-M1	synthetic	0	4.83	1.00	-0.27	this work
Glass 2	KFS-M2	synthetic	5.19	5.51	0.65	-0.27	this work
Glass 3	KFS-M3	synthetic	9.23	5.29	0.51	-0.27	this work

Note: FeO_t and MgO are in % *m/m*, #Mg is mol. MgO/(MgO + FeO_t), $\partial^{26}Mg$ (‰) was determined by solution-nebulisation MC-ICP-MS.
* Whole-rock $\partial^{26}Mg$ = -0.77‰; this work.

10^{11} Ω resistors, V/F input sensitivities up to 50 V and V/F gains of ×1 for $^{24}Mg^+$, and ×10 for $^{25}Mg^+$ and $^{26}Mg^+$. The Earth's magnetic field (EMF), able to fractionate Mg isotopes in the secondary beam (see below), was neutralised with a current of -550 mA in the Helmholtz coils surrounding the SHRIMP sample chamber. This value depends on the local EMF and must be determined empirically. To this end, we first set to 0 mA the current applied to the Helmholtz coils, centring the $^{25}Mg^+$ beam on the axial cup horizontally with the QT1 quadrupole, measuring the $^{25}Mg/^{24}Mg$ and $^{26}Mg/^{24}Mg$ ratios, moving the QT1 horizontal steering to the left by -50 bits, measuring the ratios again, moving QT1 horizontal steering to the right by 50 bits, re-measuring the ratios and comparing the three measurements. If these differed, we increased slightly the current applied to the Helmholtz coils, repeating the procedure until the three measurements matched.

Spots to be analysed were burned for about 2 min before measurements. After pre-sputtering, the secondary beam was guided horizontally and vertically to maximise the signal on the axial cup ($^{25}Mg^+$); the magnet position was fixed with a mass scan in the same cup, and the isotope ratios were measured in two sets of ten scans of 10 s each, with a total measuring time of 200 s per spot. In these conditions, the mass resolving power (M/ΔM) at 10% height was 2500 and isobaric interferences by double ions or hydrides were undetected. Small grains of the San Carlos olivine, measured every four unknowns (Hu *et al.* 2016), were used as the reference material. Data reduction was done with in-house software (available from F. Bea upon reasonable request) written in the STATA programming language. The software corrects the instrumental drift using kernel-weighted local polynomial smoothing of the isotope ratios of the measured reference material *vs.* the measurement time. It then applies the resulting function to the unknowns to compute their isotope ratios. In total, we performed 585 and 172 spot analyses of minerals and synthetic glasses, respectively (online supporting information Tables S1 and S2).

Sample preparation and SN-ICP-MS analysis

Sample digestion: Mineral particles were finely crushed in an agate mortar, then dissolved and purified using procedures previously established (Ke *et al.* 2016, Li *et al.* 2016, Gao *et al.* 2019). Garnets and other refractory minerals were digested in high-pressure bombs with concentrated HNO_3-HF (1:2 in *v/v*) in an oven at 190 °C for 48 h. The other samples were routinely dissolved in PFA beakers with concentrated HNO_3-HF (1:3 in *v/v*) at 130 °C

over 8 h. All the sample solutions were then dried and refluxed with concentrated HNO_3-HCl (1:3 in *v/v*) and HNO_3 sequentially. Finally garnets and staurolite were dissolved in 0.5 mol l^{-1} HCl-95% acetone, and other samples in 1 mol l^{-1} HNO_3, ready for purification.

Magnesium purification: Manganese-rich samples were separated from Mn in PP columns with 1 ml Bio-Rad AG50W-X8 (200–400 mesh) resin in 0.5 mol l^{-1} HCl-95% acetone, following the procedure of Gao *et al.* (2019).

The Mg cuts of garnets and staurolite were evaporated to dryness and dissolved in 100 µl 1 mol l^{-1} HNO_3. All the samples containing ~ 20 µg Mg in 100 µl 1 mol l^{-1} HNO_3 were loaded on a PFA column with 2.3 ml of Bio-Rad AG50W-X8 (200–400 mesh) resin. Matrix elements such as Na, K, Ti etc. were eluted in the first 23 ml 1 mol l^{-1} HNO_3, and Mg was then collected by 15 ml 1 mol l^{-1} HNO_3 with the other matrices remaining hosted on the resin (e.g., Ca and Al). After one purification step, most of the matrix elements were efficiently removed. To ensure the purity of the collected Mg, the same column chemistry was performed twice. Recoveries of Mg are > 99.6% for step 1 and > 99.8% for step 2 (Li *et al.* 2016, Gao *et al.* 2019). The whole procedure blank was < 10 ng and rarely reached 20–30 ng, less than 0.2% of the sample Mg processed and thus considered negligible.

Isotope measurement: Isotope measurements were conducted on a Neptune Plus MC-ICP-MS in the Isotope Geochemistry Laboratory at China University of Geosciences, Beijing, following the ^{25}Mg-^{26}Mg double spike procedure (He *et al.* 2022). Sample solutions were introduced to the plasma in 0.15 mol l^{-1} HNO_3 using a Scott double pass quartz glass spray chamber and a PFA self-aspiration micro nebuliser. ^{24}Mg, ^{25}Mg and ^{26}Mg were simultaneously collected on the L3, C and H3 Faraday cups under a low-mass resolution mode.

After measuring the concentration of each sample solution, bracketing GSB calibrator (a mono-elemental standard solution, China Iron and Steel Research Institute) and sample solutions were spiked with a ^{25}Mg-^{26}Mg double spike and prepared in 1 µg ml^{-1}, with *q* within the ±4% range of the optimised one (0.472 ± 0.02). The total ion intensity was ≥ 70 V. Each measurement consisted of a 3 s idle time and eighty cycles of 4.194 s integration time. Each analytical sequence for each sample was repeated four times. A set of under-spiked and over-spiked GSB standard solutions, with *q* ranging from 0.452, 0.462, 0.482 to 0.492, were analysed in each sequence to correct the inaccuracy arising from preparation of the critical mixtures. The Mg isotope ratios are reported as δ values relative to DSM-3:

$$\delta^{26}Mg_{DMS-3} = \delta^{26}Mg_{GSB} + \delta^{26}Mg_{DSM-3}(GSB) + \delta^{26}Mg_{GSB} \times \delta^{26}Mg_{DSM-3}(GSB) \quad (4)$$

where $\delta^{26}Mg_{DSM-3}(GSB)$ is -2.032 ± 0.038‰ (2s, $N = 225$; (Gao *et al.* 2019). The uncertainty is two standard error of the mean ($2s/\sqrt{n}$), *n* refers to the number of times of a single isotope measurement. Analyses of BHVO-2 and BCR-2 from USGS processed through column chemistry, yielded $\delta^{26}Mg$ = -0.19 ± 0.01‰ for BHVO-2 and $\delta^{26}Mg$ = -0.19 ± 0.04‰ for BCR-2, identical to the literature data within analytical uncertainty (He *et al.* 2022).

Results and discussion

As mentioned, SIMS analysis causes a variably intense instrumental mass fractionation of Mg isotopes. Given that the secondary beam arising from different minerals is unlikely to behave differently during the flight from the source slit to the magnet and the detectors, the IMF should occur within the sample chamber, be it related to the sputtering process or the extraction and subsequent guidance of the secondary beam to the source slit, or both.

During sputtering, one of the main factors able to fractionate isotopes of the same element is the force constant difference between the bonds linking the isotopes of the studied element to the mineral lattice, $\Delta F = F_{hard} - F_{soft}$. Coordination sites with "soft" bonds tend to be preferentially populated with the 'lightest' isotopes, whereas those with "hard" bonds do it with the heaviest ones (e.g., Albarède 2009, p. 53). On collision with primary ions, mineral species with different ΔF but the same $^{25}Mg/^{24}Mg$ and $^{26}Mg/^{24}Mg$ will release ions of the three isotopes at different rates, thus yielding different isotope ratios that will depend on how the force constant differences of reference material and unknowns compare.

Magnesium isotopes have also shown noticeable IMF when reference materials and minerals belonging to the same mineral species have different chemical compositions, such as often happens in solid solutions between Mg and Fe end-members (e.g., Kita *et al.* 2012, Luu *et al.* 2013, Ushikubo *et al.* 2013, Fukuda *et al.* 2020, Richter *et al.* 2021, etc.). This effect might arise because (i) the concentration of Fe ions affects the distribution of Mg isotope ions between bonds of different force constants, (ii) the variable composition of the ion cloud affects the ionisation efficiency of each isotope

differently, or (iii) the variable composition of the ion cloud affects the flight path of the Mg isotopes from the mineral surface to the source slit. As illustrated below, the last hypothesis seems more likely, especially if the effects of the Earth's magnetic field on the ion flight paths are not corrected.

Correction of Earth's magnetic field and the effects of variable chemical composition

The Earth's magnetic field causes $^{24}Mg^+$, $^{25}Mg^+$ and $^{26}Mg^+$ to follow somewhat divergent horizontal trajectories from the sputtered spot to the source slit, which, being narrower than the secondary beam, truncates each isotope differently (Figure 2a). Consequently, minor variations in the secondary beam trajectory will cause intolerable variations in the measured isotope ratios. In the SHRIMP, the EMF effects can be amended using two horizontal Helmholtz coils surrounding the sample chamber, one above and the other below the secondary beam plane. When the magnetic field created by the current applied to the coils (see above, *Sample preparation and SHRIMP analysis*) compensates for the local EMF, the three Mg isotopes do not diverge (Figure 2b), thus being equally truncated by the source slit. In this situation, minor shifts in the secondary beam trajectory would have little or no effect on the measured isotope ratios.

These shifts may arise from small errors in the guidance lenses during the pre-analysis adjustments; if so, they will occur randomly without correspondence to the chemical composition. Minor but still perceptible variations in the trajectory of Mg ions might also arise from interaction with variable amount of Fe ions within the ionic cloud resulting from sputtering. To check this idea, we used the three synthetic glasses with the same Mg isotope composition but different Mg/Fe ratio (Table 1). We ran two measurement sessions, with and without EMF correction. Each session consisted of thirty spots of randomly interspersed fragments of each glass plus the San Carlos olivine as reference material measured every four unknowns. Measurement results are shown in Figure 3 and given in Table S2.

The measurements with no EMF correction show large dispersions and the replicates of each material plot along slightly curved and steeper-than-TFL alignments (Figure 3a). Each glass alignment cuts the TFL at different points, the coordinates of which increase with the glass iron content, thus indicating a compositional effect. In contrast, the EMF-corrected measurements plot perfectly aligned to the TFL yielding less dispersion, and the means of the three glasses cannot be distinguished statistically (p-value > 0.14, Table 2). These data suggest that the glasses' bulk compositions affected Mg isotope ratios only when the EMF was not properly neutralised. Given that there is no reason for not expanding this conclusion to minerals, we thus accept as a working hypothesis that the extensive IMF caused by the SHRIMP, either in single-collector or in multiple-collector when the EMF is adequately corrected, does not depend on the chemical composition but primarily relates to the different structures of reference

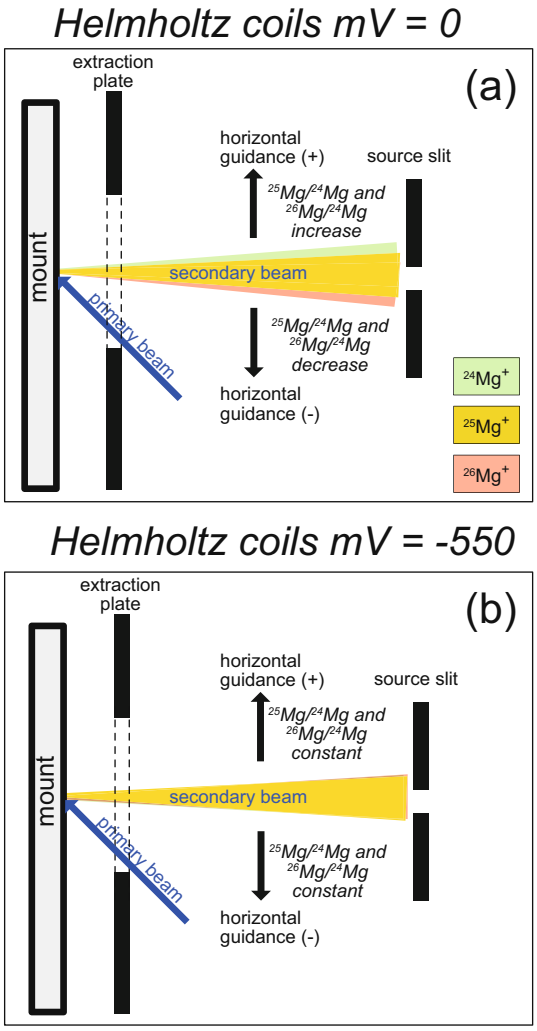

Figure 2. (a) Trajectories of $^{24}Mg^+$, $^{25}Mg^+$ and $^{26}Mg^+$ from the sample surface to the source slit. The Earth's magnetic field (EMF) can cause divergent trajectories, so the source slit truncates each isotope beam differently. Therefore, small variations in the secondary beam horizontal guidance will cause intolerable errors in the isotope ratio measurements. (b) If the Helmholtz coils are activated, the EMF can be compensated, eliminating the divergence and improving the results. The current applied to the Helmholtz coils depends on the local magnetic field.

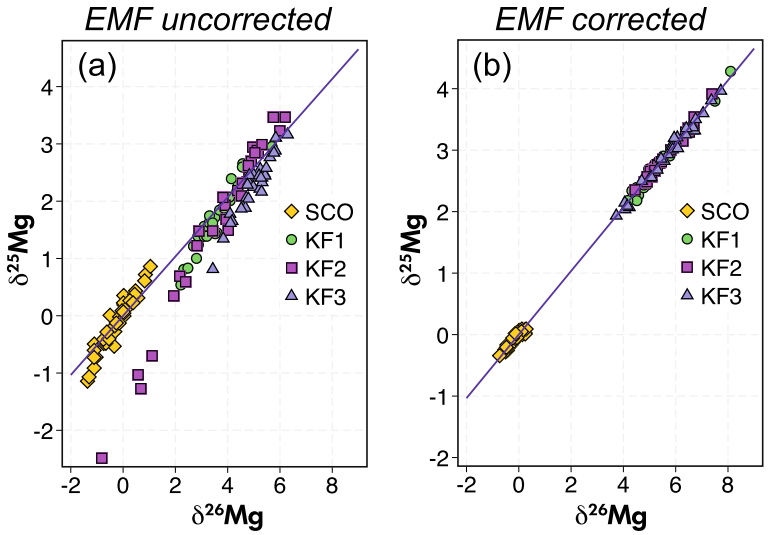

Figure 3. The three synthetic glasses measured with the EMF corrected and uncorrected. When the EMF is corrected, the three glasses plot along the terrestrial fractionation line (TFL) and yield statistically indistinguishable δ^{25}Mg and δ^{26}Mg means despite the large compositional difference (see Tables 1 and 3). When the EMF is uncorrected, neither the glasses nor the San Carlos Olivine plot along the TFL, the replicates' variation increases greatly, and the three glasses intersect the TFL at coordinates increasing with the glass iron concentration. See text for details.

Table 2.
Two-sample *t*-test with unequal variances comparing the mean ∂^{25}Mg of the glasses with no FeO (KM1), 5% FeO (KM2) and 10% *m/m* FeO (KM3) measured with the EFM corrected; we did not find a statistically significant difference in the means of ∂^{25}Mg. The same occurred with ∂^{26}Mg

Glass	Obs	Mean	Std. err.	Std. dev.	[95% conf. interval]
KM1	25	2.740186	0.1102911	0.5514553	2.512556 / 2.967815
KM2	30	2.909161	0.066679	0.3652162	2.772787 / 3.045535
Combined	55	2.832354	0.062377	0.4625999	2.707296 / 2.957412
diff		-0.1689751	0.1288806		-0.429393 / 0.091442
diff = mean(KM1) - mean(KM3);		Satterthwaite's degrees of freedom = 40.2956;			*t* = -1.3111
Ha: diff < 0			Ha: diff!= 0		Ha: diff > 0
Pr(T < t) =	0.0986	**Pr(|T| > |t|) = 0.1972**	Pr(T > t) = 0.9014		
Glass	**Obs**	**Mean**	**Std. err.**	**Std. dev.**	**[95% conf. interval]**
KM1	25	2.740186	0.1102911	0.5514553	2.512556 / 2.967815
KM3	30	2.960198	0.1006689	0.5421184	2.753988 / 3.166409
Combined	54	2.858341	0.0751829	0.552479	2.707543 / 3.009138
diff	-0.2200128	0.1493263	-0.5198605 / 0.079834		
diff = mean(KM1) - mean(KM3);		Satterthwaite's degrees of freedom = 50.5651;			*t* = -1.4734
Ha: diff < 0			Ha: diff!= 0		Ha: diff > 0
Pr(T < t) =	0.0734	**Pr(|T| > |t|) = 0.1468**	Pr(T > t) = 0.9266		
Glass	**Obs**	**Mean**	**Std. err.**	**Std. dev.**	**[95% conf. interval]**
KM2	30	2.909161	0.066679	0.3652162	2.772787 / 3.045535
KM3	30	2.960198	0.1006689	0.5421184	2.753988 / 3.166409
Combined	54	2.934247	0.059551	0.4574197	2.815043 / 3.053451
diff	-0.0510377	0.120749	-0.2937076 / 0.191632		
diff = mean(KM1) - mean(KM3);		Satterthwaite's degrees of freedom = 50.5651:			*t* = -1.4734
H0: diff = 0					
Ha: diff < 0			Ha: diff!= 0		Ha: diff > 0
Pr(T < t) =	0.3372		**Pr(|T| > |t|) = 0.6744**		Pr(T > t) = 0.6628

Table 3.
Raw mean SHRIMP measurement results of the studied minerals (the full dataset is given in online supporting information Table S1). Note the large range of values, much higher than the SN-MC-ICP-MS data shown in Table 1

ID	Spots	$^{25}Mg/^{24}Mg$	1*s*	$^{26}Mg/^{24}Mg$	1*s*	$\delta^{25}Mg$	1*s*	$\delta^{26}Mg$	1*s*
OLsc	59	0.126836	0.000011	0.139763	0.000025	-0.12	0.09	-0.24	0.18
OPXsc	30	0.126954	0.000021	0.140015	0.000047	0.81	0.17	1.57	0.33
CPXsc	30	0.126958	0.000024	0.140023	0.000057	0.85	0.19	1.62	0.41
SPsc	30	0.126207	0.000028	0.138383	0.000059	-5.08	0.22	-10.11	0.42
OLro	17	0.12681	0.000058	0.139692	0.000169	-0.33	0.46	-0.74	1.21
OPXro	22	0.126938	0.000028	0.139984	0.000066	0.68	0.22	1.34	0.47
CPXro	23	0.126972	0.000022	0.140064	0.000053	0.95	0.17	1.92	0.38
SPro	19	0.126229	0.000021	0.138468	0.000054	-4.91	0.16	-9.5	0.39
OLas	30	0.126794	0.000038	0.139667	0.000079	-0.46	0.3	-0.92	0.56
OPXas	24	0.126927	0.000019	0.139956	0.000042	0.6	0.15	1.14	0.3
CPXas	29	0.126924	0.000017	0.139939	0.000038	0.57	0.14	1.02	0.27
AMPas	30	0.126883	0.000025	0.139876	0.000058	0.25	0.19	0.57	0.41
OLf	24	0.126848	8E-06	0.139791	0.000016	-0.03	0.06	-0.04	0.11
CRD	26	0.127228	0.000027	0.140597	0.000041	2.97	0.21	5.73	0.3
ACN	30	0.126933	0.000029	0.13997	0.000063	0.64	0.23	1.25	0.45
OPX7	25	0.126945	0.000033	0.139996	0.000083	0.74	0.26	1.43	0.59
CPX2	31	0.12687	0.000018	0.139837	0.000038	0.15	0.14	0.29	0.27
GRTf	37	0.126945	0.000061	0.139995	0.000062	0.74	0.48	1.42	0.44
BIOV35	18	0.126842	0.000024	0.139797	0.000034	-0.08	0.19	0.01	0.25

materials and minerals. This idea finds support from the fact that olivines with Fo_{90} (from a peridotite) and Fo_{68} (from a mafic granulite) measured correcting the EMF yielded $\delta^{26}Mg$ values that differ by 0.68‰ (Table 3), and this variation probably arises from the bulk composition differences of their respective host rocks, $\delta^{26}Mg \approx$ -0.24‰ in the San Carlos peridotite (mean of mineral compositions reported by Hu *et al.* 2016) and $\delta^{26}Mg \approx$ -0.77‰ in the mafic granulite (Table 3).

Figure 3b also shows that the EMF-corrected analyses still have some dispersion along the TFL, which is prominent in the glasses but still perceptible in the San Carlos olivine. In the glasses, this phenomenon probably reflects the presence of variable amounts of small crystallites (< 1 μm) within the analysed spot. In the minerals, however, the variation must stem from another reason. Excluding variations in the chemical composition because the dispersion happens in all minerals, even those remarkably homogeneous, the most plausible explanations are lattice anisotropy, isotopic heterogeneity or fluctuations in the sputter rate caused by variable primary beam intensity. In most cases, mineral structures are anisotropic; thus, it is logical that the intensity of the matrix effects related to the structure and, hence, the sputtering rate might vary with the crystallographic orientation of the analysed grains. Isotopic heterogeneities would cause the same effect; however, the fact that different specimens of the same mineral, even those equilibrated at 1000 °C, always yield similar dispersion favours the idea of structural anisotropy (constant) over isotopic heterogeneity (variable). Independently of the particular reason, this effect causes the error averaging analyses of the same mineral to always be much higher than the error of every single analysis; accordingly, to get a reasonably representative isotope composition of each mineral requires the analysis of at least twenty replicates.

Analyses of minerals and calculation of IMF correction factors

The minerals studied include olivine, clinopyroxene, orthopyroxene, amphibole, spinel, garnet, cordierite and biotite; in this set, MgO ranges from 3 to 50% *m/m*, mol. MgO/(FeO+MgO) from 0.13 to 0.92, and $\delta^{26}Mg$ (SN-MC-ICP-MS) from -1.88 to 0.28 (Table 1). Raw SHRIMP data (drift and EMF corrected) show a more considerable $\delta^{26}Mg$ variation, from -10.1 to 5.7 (Table 3), with spinel and cordierite having the lowest and the highest values, respectively (Figure 4). Amphibole and biotite have Mg isotope ratios comparable to olivine; pyroxenes and garnet are moderately enriched in heaviest isotopes. In the three-isotope diagram (Figure 4), the raw data means of all analysed minerals fit well (R = 0.9998) on a straight line identical to the TFL. The slope – calculated by robust regression – is ß = 0.517, thus matching the Rayleigh fractionation line (Davis *et al.* 2015) and intermediate between the kinetic and equilibrium fractionation lines calculated by Young and Galy (2004).

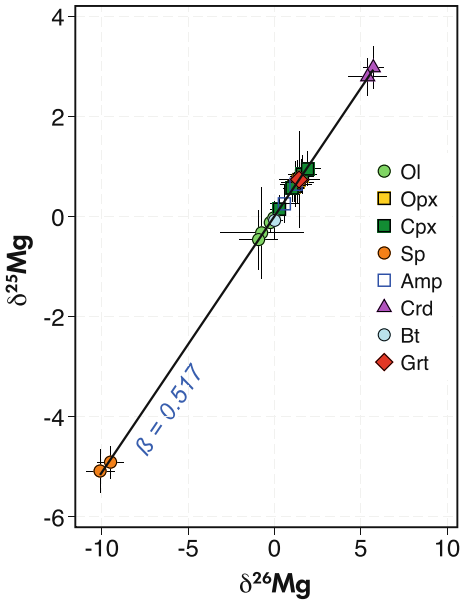

Figure 4. The SHRIMP results on the three-isotope diagram plot along the TFL. The mean δ^{25}Mg and δ^{26}Mg yielded a correlation coefficient *R* = 0.9998 with a slope ß = 0.517, characteristic of the Rayleigh mass fractionation law. The crosses represent 2*s*. Note the wide dispersion along the TFL, δ^{26}Mg from -9.7 to 5.9, much higher than the SA-MC-ICP-MS analyses of the same minerals, δ^{26}Mg from 1.88 to 0.26, Tables 1 and 2. Cordierite and spinel occupy the heavier and lighter isotope-enriched extremes, respectively. The large variation along the TFL is caused by structural differences between the reference material (San Carlos olivine) and the other minerals. See text.

From the raw data, we calculated IMF correction factors using two different approaches (Table 4): (i) based on the San Carlos olivine: $^{25}F_{ol}$ = (^{25}Mg/^{24}Mg$_{mineral}$)/(^{25}Mg/^{24}Mg$_{SC\ olivine}$), (ii) based on SHRIMP to SN-MC-ICP-MS ratios: $^{25}F_{tm}$ = (^{25}Mg/^{24}Mg $_{SHRIMP}$)/(^{25}Mg/^{24}Mg $_{SN\text{-}MC\text{-}ICP\text{-}MS}$), where subscripts "*ol*" and "*tm*" stand for "*olivine*" and "*two methods*", respectively. We used the San Carlos olivine as the SHRIMP calibration material but any other well-known mineral can be used equally.

The two methods yielded similar values: plotting $^{25}F_{tm}$ against $^{25}F_{ol}$ for each analysed specimen yields a regression line with slope =1 and correlation coefficient of 0.993 (Figure 5). This excellent correspondence is most remarkable because the $^{25}F_{ol}$ coefficients result from comparing the San Carlos olivine (#Mg = 0.90) with minerals with very different composition (#Mg from 0.92 to 0.13), whereas the $^{25}F_{tm}$ coefficients arise from two different measurements on the same mineral concentrate. The coefficients are also robust because different specimens of a given mineral yield the same values independently of the specimen composition. These observations confirm that if the EMF is adequately corrected, the matrix effects overwhelmingly depend on the mineral structure.

Although the two types of coefficients are similar, we preferred the $^{25}F_{tm}$ ones (Table 4) because being based on two independent methods seems less prone to errors. The matrix-correction factor for ^{26}Mn/^{24}Mg are calculated as $^{26}F_{tm} = 1 + (^{25}F_{tm} - 1)/0.517$.

We tested the IMF correction factors' efficacy in (i) the Ronda peridotite minerals, also measured by SN-MC-ICP-MS but not included in the F_{tm} calculations to avoid tautologies, and (ii) the minerals of the high-*T* mafic granulite, not measured in that way, but probably isotopically homogeneous because of diffusion (Table 5). The SHRIMP IMF-corrected and the SN-MC-ICP-MS values of Ronda minerals differ by less than 0.3‰, except for the slightly serpentinised olivine, which differs by 0.52‰ probably because the ablated spot contained olivine partially transformed to serpentine, the structural effects of which differ from olivine. The minerals of the mafic granulite, which uncorrected vary from more than 2‰, yielded corrected δ^{26}Mg in the range -0.64‰ to -0.97‰, i.e., within 0.3‰ and enclosing the SN-MC-ICP-MS bulk rock analysis, δ^{26}Mg = -0.77‰, thus suggesting the F_{tm}-based correction worked.

Table 6 summarises the recommended matrix correction coefficients. They must be considered provisional and amenable to improvement as more data become available, especially those based on a single specimen (garnet, biotite, cordierite).

Conclusions

- The multi-collector SHRIMP microprobe can quickly and precisely measure Mg isotopes in geologically fractionated materials despite the large differences in instrumental mass fractionation (IMF) between minerals inherent to the system.

- The IMF is mostly related to the force constant difference between the bonds linking the isotopes of the studied element to the mineral lattice, that is, the mineral structure and not to the chemical composition, provided the local Earth magnetic field (EMF) is adequately compensated.

- Uncompensated EMF causes the $^{24}Mg^+$, $^{25}Mg^+$ and $^{26}Mg^+$ trajectories within the sample chamber to diverge so

Table 4.
Matrix-correction factors. $^{25}Mg/^{24}Mg^{*}$ and $^{25}Mg/^{24}Mg^{**}$ represent raw SHRIMP data and SN-MC-ICP-MS measurements, respectively. Factors $^{25}F_{ol}$ resulted from dividing each data in the SHRIMP column by the San Carlos olivine, 0.126836. Factors $^{25}F_{tm}$ resulted from dividing the SHRIMP data by the corresponding ICP-MS data of each mineral

ID	$^{25}Mg/^{24}Mg^{*}$	1 *s*	$^{25}F_{ol}$	Error	$^{25}Mg/^{24}Mg^{**}$	$^{25}F_{tm}$	Error
OLsc	0.126836	0.000011	1.000000	0.000000	0.126835	1.000000	0.000011
OPXsc	0.126954	0.000021	1.000928	0.000079	0.126837	1.000922	0.000069
CPXsc	0.126958	0.000024	1.000965	0.000102	0.126836	1.000964	0.000091
SPsc	0.126207	0.000028	0.995037	0.000130	0.126843	0.994979	0.000119
OLro	0.126810	0.000058	0.999794	0.000367	0.126837	0.999788	0.000357
OPXro	0.126938	0.000028	1.000804	0.000130	0.126837	1.000793	0.000119
CPXro	0.126972	0.000022	1.001071	0.000083	0.126842	1.001024	0.000072
SPro	0.126229	0.000021	0.995214	0.000074	0.126870	0.994951	0.000063
OLas	0.126794	0.000038	0.999665	0.000208			
OPXas	0.126927	0.000019	1.000717	0.000057			
CPXas	0.126924	0.000017	1.000691	0.000047			
AMPas	0.126883	0.000025	1.000374	0.000106			
OLf	0.126848	0.000008	1.000093	0.000026	0.126837	1.000082	0.000037
CRD	0.127228	0.000027	1.003093	0.000122	0.126816	1.003253	0.000111
CAN	0.126933	0.000029	1.000765	0.000139	0.126832	1.000800	0.000128
OPX7	0.126945	0.000033	1.000859	0.000174	0.126807	1.001086	0.000163
CPX2	0.126870	0.000018	1.000266	0.000052	0.126728	1.001120	0.000041
GRTf	0.126945	0.000061	1.000859	0.000392	0.126761	1.001449	0.000381
BT35	0.126842	0.000024	1.000043	0.000100	0.126844	0.999980	0.000089

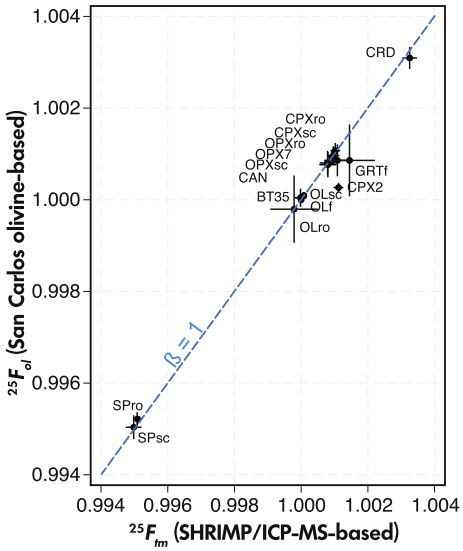

Figure 5. Plot of the olivine-based against the two methods-based IMF correction factors. The two kinds of independently calculated correction factors show excellent correspondence, with a correlation coefficient of $R = 0.993$, thus suggesting the robustness of the correction.

that the source slit truncates them differently. Under these conditions, minor changes in the secondary beam guidance result in huge variations in the measured isotope ratios. The guidance fluctuations may arise from aleatory errors in the secondary beam-positioning lens or because of the variable composition of the ionic cloud resulting from sputtering.

- In the SHRIMP, the EMF was compensated by applying an empirically determined current to two horizontal Helmholtz coils, one above and the other below the plane of the secondary beam. The compensation prevented the ionic paths from diverging, thus cancelling the effects of the secondary beam guidance on the measured isotope ratios. With the EMF adequately compensated, each mineral species causes constant IMF effects, which can be easily corrected by applying suitable fractionation coefficients.

- The standard error measuring Mg isotope ratios in a single spot was typically around 0.007%, whereas the point-to-point error on approximately twenty analyses of a very homogeneous mineral such as San Carlos olivine was always larger, about 0.013%. We attributed this effect to the anisotropy of the mineral lattice.

- Mineral mass-fraction factors can be calculated in two ways: from mineral-to-reference material ratios measured in the same session (here, we used the San Carlos olivine as reference material) or based on the SHRIMP to SN-MC-ICP-MS ratios of the same minerals. These permit correction of the instrumental mass-fractionation caused by the SHRIMP within a ≈ 0.3‰ error range, which may be considered the method's accuracy.

Table 5.
Application of the matrix-correction factors. $^{26}F_{tm}$ was calculated as 1 + ($^{25}F_{tm}$ - 1)/0.517. The rightmost column reflects the difference between δ^{26}Mg calculated from the SN-MC-ICP-MS and the corrected SHRIMP data. Note how all data, except the Ronda olivine, differ by less than 0.3‰. The Ronda olivine is slightly serpentinised, which may have affected its structure-related mass fractionation. See text for details

	Raw SHRIMP values				Correction factors		Corrected SHRIMP values				SN-MC-ICP-MS		
ID	$^{25}Mg/^{24}Mg$	$^{26}Mg/^{24}Mg$	$\delta^{25}Mg$	$\delta^{26}Mg$	$^{25}F_{tm}$	$^{26}F_{tm}$	$^{25}Mg/^{24}Mg$	$^{26}Mg/^{24}Mg$	$\delta^{25}Mg$	$\delta^{26}Mg$	$\delta^{25}Mg$	$\delta^{26}Mg$	Difference
OLsc	0.1268360	0.1397625	-0.12	-0.24	1.00000	1.00000	0.126836	0.139763	-0.12	-0.24	-0.12	-0.24	0.00
OPXsc	0.1269537	0.1400153	0.81	1.57	1.00093	1.00181	0.126835	0.139763	-0.13	-0.24	-0.11	-0.22	0.02
CPXsc	0.1269584	0.1400230	0.84	1.62	1.00104	1.00200	0.126827	0.139743	-0.19	-0.38	-0.12	-0.23	0.15
SPsc	0.1262065	0.1383834	-5.08	-10.1	0.99498	0.99029	0.126843	0.139740	-0.06	-0.40	-0.12	-0.23	0.17
OLro	0.1268099	0.1396922	-0.33	-0.74	1.00000	1.00000	0.126810	0.139692	-0.33	-0.74	-0.11	-0.22	0.52
OPXro	0.1269380	0.1399839	0.68	1.34	1.00093	1.00181	0.126820	0.139731	-0.25	-0.46	-0.11	-0.21	0.25
CPXro	0.1269719	0.1400643	0.95	1.92	1.00104	1.00200	0.126841	0.139784	-0.08	-0.08	-0.07	-0.14	-0.06
SPro	0.1262290	0.1384683	-4.91	-9.5	0.99497	0.99026	0.126868	0.139830	0.13	0.24	0.14	0.28	0.04
OLas	0.1267935	0.1396672	-0.46	-0.92	1.00000	1.00000	0.126794	0.139667	-0.45	-0.92			
OPXas	0.1269270	0.1399556	0.6	1.14	1.00093	1.00181	0.126809	0.139703	-0.34	-0.66			
CPXas	0.1269237	0.1399391	0.57	1.02	1.00104	1.00200	0.126792	0.139659	-0.46	-0.98			
AMPas	0.1268834	0.1398763	0.25	0.57	1.00080	1.00155	0.126782	0.139660	-0.55	-0.97			
OLfer	0.1268478	0.1397905	-0.03	-0.04	1.00000	1.00000	0.126848	0.139791	-0.03	-0.04	-0.11	-0.21	-0.17
CORD	0.1272283	0.1405966	2.97	5.73	1.00325	1.00629	0.126816	0.139717	-0.28	-0.56	-0.28	-0.54	0.02
CANN	0.1269330	0.1399703	0.64	1.25	1.00080	1.00155	0.126832	0.139754	-0.15	-0.30	-0.16	-0.30	0.00
OPX7	0.1269450	0.1399957	0.74	1.43	1.00093	1.00181	0.126827	0.139743	-0.19	-0.38	-0.35	-0.67	-0.29
CPX2	0.1268698	0.1398367	0.15	0.29	1.00104	1.00200	0.126739	0.139557	-0.89	-1.71	-0.97	-1.88	-0.17
GRTf	0.1269450	0.1399952	0.74	1.42	1.00145	1.00280	0.126761	0.139604	-0.71	-1.37	-0.71	-1.37	0.00
BIOV35	0.1268415	0.1397972	-0.08	0.01	0.99998	0.99996	0.126844	0.139803	-0.06	0.05	-0.06	-0.11	-0.16

Table 6.
Recommended matrix correction coefficients. The last column contains the values Ireland *et al.* (1982) determined with the SHRIMP-I, recalculated to be olivine-based instead of kaersutite-based. The authors did not specify whether the pyroxene was ortho- or clinopyroxene. Note the good correspondence with our $^{25}F_{tm}$ factors

Phase	$^{25}F_{tm}$	$^{26}F_{tm}$	$^{25}F^*$
olivine	1.00000	1.00000	1.00000
orthopyroxene	1.00093	1.00181	1.00147
clinopryroxene	1.00104	1.00200	1.00147
spinel	0.99497	0.99026	0.99484
amphibole	1.00080	1.00155	1.00103
cordierite	1.00325	1.00629	
biotite	0.99998	0.99996	
garnet	1.00145	1.00280	

• The correction factors permit analysing different mineral species of variable composition with a single mineral as a reference material, thus simplifying the routine measurement of Mg isotopes in minerals and expanding their applicability to Earth Sciences.

Acknowledgements

The authors have benefitted enormously from the corrections made by two anonymous referees. This work has been financially supported by the Andalucian-FEDER grant P18-FR-1696, and the Spanish grant PID2020-114872GB-I00. It is the IBERSIMS publication No. 106.

Scientific editing by Paul J. Sylvester.

Data availability statement

The data that support the findings of this study are available in the supplementary material of this article.

References

Albarède F. (2009)
Geochemistry. An introduction (2nd edition). **Cambridge University Press (Cambridge)**, 342pp.

Catanzaro E.J., Murphy T.J., Garner E.L. and Shields W.R. (1966)
Absolute isotopic abundance ratios and atomic weight of magnesium. **Journal of Research of the National Bureau of Standards, 70A**, 453–458.

references

Chaussidon M., Deng Z., Villeneuve J., Moureau J., Watson B., Richter F. and Moynier F. (2017)
In situ analysis of non-traditional isotopes by SIMS and LA-MC-ICP-MS: Key aspects and the example of Mg isotopes in olivines and silicate glasses. Reviews in Mineralogy and Geochemistry, 82, 127–163.

Davis A.M., Richter F.M., Mendybaev R.A., Janney P.E., Wadhwa M. and McKeegan K.D. (2015)
Isotopic mass fractionation laws for magnesium and their effects on ^{26}Al–^{26}Mg systematics in solar system materials. Geochimica et Cosmochimica Acta, 158, 245–261.

Fukuda K., Beard B.L., Dunlap D.R., Spicuzza M.J., Fournelle J.H., Wadhwa M. and Kita N.T. (2020)
Magnesium isotope analysis of olivine and pyroxene by SIMS: Evaluation of matrix effects. Chemical Geology, 540, 119482.

Galy A., Belshaw N.S., Halicz L. and O'Nions R.K. (2001)
High-precision measurement of magnesium isotopes by multiple-collector inductively coupled plasma-mass spectrometry. International Journal of Mass Spectrometry, 208, 89–98.

Galy A., Yoffe O., Janney P.E., Williams R.W., Cloquet C., Alard O., Halicz L., Wadhwa M., Hutcheon I.D., Ramon E. and Carignan J. (2003)
Magnesium isotope heterogeneity of the isotopic standard SRM980 and new reference materials for magnesium-isotope-ratio measurements. Journal of Analytical Atomic Spectrometry, 18, 1352–1356.

Gao T., Ke S., Li R.Y., Meng X.N., He Y. S Liu C., Wang Y., Li Z. and Zhu J.M. (2019)
High-precision magnesium isotope analysis of geological and environmental reference materials by multiple-collector inductively coupled plasma-mass spectrometry. Rapid Communications in Mass Spectrometry, 33, 767–777.

Garrido C.J., Gueydan F., Booth-Rea G., Precigout J., Hidas K., Padrón-Navarta J.A. and Marchesi C. (2011)
Garnet lherzolite and garnet-spinel mylonite in the Ronda peridotite: Vestiges of Oligocene backarc mantle lithospheric extension in the western Mediterranean. Geology, 39, 927–930.

Gray C.M. and Compston W. (1974)
Excess ^{26}Mg in the Allende meteorite. Nature, 251, 495–497.

He Y.S., Sun A.Y., Zhang Y.C., Yang R.Y., Ke S., Wang Y. and Teng F.Z. (2022)
High-precision and high-accuracy magnesium isotope analysis on multiple-collector inductively coupled plasma-mass spectrometry using a critical mixture double spike technique. Solid Earth Sciences, 7, 188–199.

Hu Y., Harrington M.D., Sun Y., Yang Z., Konter J. and Teng F.Z. (2016)
Magnesium isotopic homogeneity of San Carlos olivine: A potential standard for Mg isotopic analysis by multi-collector inductively coupled plasma-mass spectrometry. Rapid Communications in Mass Spectrometry, 30, 2123–2132.

Hutcheon I.D., Steele I.M., Smith J.V. and Clayton R.N. (1978)
Ion microprobe, electron microprobe and cathodoluminescence data for Allende inclusions with emphasis on plagioclase chemistry. 9th Lunar and Planetary Science Conference (Houston, Texas), Proceedings, 1, 1345–1368.

Ickert R., Hiess J., Williams I., Holden P., Ireland T., Lanc P., Schram N., Foster J. and Clement S. (2008)
Determining high precision, *in situ*, oxygen isotope ratios with a SHRIMP II: Analyses of MPI-DING silicate-glass reference materials and zircon from contrasting granites. Chemical Geology, 257, 114–128.

Ireland T.R., Compston W. and Esat T.M. (1986)
Magnesium isotopic compositions of olivine, spinel, and hibonite from the Murchison carbonaceous chondrite. Geochimica et Cosmochimica Acta, 50, 1413–1421.

Ke S., Teng F.Z., Li S.G., Gao T., Liu S.A., H. and Mo X. (2016)
Mg, Sr, and O isotope geochemistry of syenites from northwest Xinjiang, China: Tracing carbonate recycling during Tethyan oceanic subduction. Chemical Geology, 436, 1109–1119.

Kita N.T., Ushikubo T., Knight K.B., Mendybaev R.A., Davis A.M., Richter F.M. and Fournelle J.H. (2012)
Internal ^{26}Al–^{26}Mg isotope systematics of a Type B CAI: Remelting of refractory precursor solids. Geochimica et Cosmochimica Acta, 86, 37–51.

Lee T. and Papanastassiou D.A. (1974)
Mg isotopic anomalies in the Allende meteorite and correlation with O and Sr effects. Geophysical Research Letters, 1, 225–228.

Li R.Y., Ke S., He Y. S, Gao T. and Meng X.N. (2016)
High precision magnesium isotope measurement for high-Cr samples. Bulletin Mineralogy, Petrology and Geochemistry, 35, 441–447.

Luu T.-H., Chaussidon M., Mishra R.K., Rollion-Bard C., Villeneuve J., Srinivasan G. and Birck J.-L. (2013)
High precision Mg isotope measurements of meteoritic samples by secondary ion mass spectrometry. Journal of Analytical Atomic Spectrometry, 28, 67–76.

Molina J.F., Bea F., Montero P., Haissen F., González-Lodeiro F., Errami A., Sadki O., Moreno J.A., Cambeses A. and Mouttaqi A. (2018)
High-P amphibolite-facies metamorphism in the Adrar–Souttouf Metamafic Complex, Oulad Dlim Massif (West African Craton margin, Morocco). Comptes Rendus Geoscience, 350, 245–254.

Richter F., Saper L.M., Villeneuve J., Chaussidon M., Watson E.B., Davis A.M., Mendybaev R.A. and Simon S.B. (2021)
Reassessing the thermal history of Martian meteorite Shergotty and Apollo mare basalt 15555 using kinetic isotope fractionation of zoned minerals. Geochimica et Cosmochimica Acta, 295, 265–285.

references

Richter F.M., Davis A.M., Ebel D.S. and Hashimoto A. (2002)
Elemental and isotopic fractionation of Type B calcium-, aluminum-rich inclusions: Experiments, theoretical considerations, and constraints on their thermal evolution. **Geochimica et Cosmochimica Acta**, **66**, 521–540.

Russell S.S., Davis A.M., Macpherson G.J., Guan Y. and Huss G.R. (2000)
Refractory inclusions from the ungrouped carbonaceous chondrites MacAlpine Hills 87300 and 88107. **Meteoritics and Planetary Science**, **35**, 1051–1066.

Ushikubo T., Nakashima D., Kimura M., Tenner T.J. and Kita N.T. (2013)
Contemporaneous formation of chondrules in distinct oxygen isotope reservoirs. **Geochimica et Cosmochimica Acta**, **109**, 280–295.

Young E.D. and Galy A. (2004)
The isotope geochemistry and cosmochemistry of magnesium. **Reviews in Mineralogy and Geochemistry**, **55**, 197–230.

Supporting information

The following supporting information may be found in the online version of this article:

Table S1. Complete set of SHRIMP measurement results for magnesium isotope ratios of the studied minerals.

Table S2. Magnesium isotope ratio measurement results for EMF corrected and uncorrected conditions.

This material is available from: http://onlinelibrary.wiley.com/doi/10.1111/ggr.12547/abstract (This link will take you to the article abstract).